BIOCHEMISTRY
including biophysical chemistry & molecular biology

Article

pubs.acs.org/biochemistry

Kinetics of Myosin Light Chain Kinase Activation of Smooth Muscle Myosin in an *in Vitro* Model System

Feng Hong,[†] Kevin C. Facemyer,[†] Michael S. Carter,[†] Del R. Jackson,[†] Brian D. Haldeman,[†] Nick Ruana,[†] Cindy Sutherland,[‡] Michael P. Walsh,[‡] Christine R. Cremo,[†] and Josh E. Baker*[,†]

[†]Department of Biochemistry and Molecular Biology, University of Nevada School of Medicine, Reno, Nevada 99557, United States

[‡]Department of Biochemistry and Molecular Biology, University of Calgary Faculty of Medicine, 3280 Hospital Drive Northwest, Calgary, Alberta, T2N 4N1 Canada

Supporting Information

ABSTRACT: During activation of smooth muscle contraction, one myosin light chain kinase (MLCK) molecule rapidly phosphorylates many smooth muscle myosin (SMM) molecules, suggesting that muscle activation rates are influenced by the kinetics of MLCK−SMM interactions. To determine the rate-limiting step underlying activation of SMM by MLCK, we measured the kinetics of calcium-calmodulin (Ca^{2+}CaM)−MLCK-mediated SMM phosphorylation and the corresponding initiation of SMM-based F-actin motility in an *in vitro* system with SMM attached to a coverslip surface. Fitting the time course of SMM phosphorylation to a kinetic model gave an initial phosphorylation rate, k_p^o, of ∼1.17 heads s^{-1} $MLCK^{-1}$. Also, we measured the dwell time of single streptavidin-coated quantum dot-labeled MLCK molecules interacting with surface-attached SMM and phosphorylated SMM using total internal reflection fluorescence microscopy. From these data, the dissociation rate constant from phosphorylated SMM was 0.80 s^{-1}, which was similar to the k_p^o mentioned above and with rates measured in solution. This dissociation rate was essentially independent of the phosphorylation state of SMM. From calculations using our measured dissociation rates and K_d values, and estimates of SMM and MLCK concentrations in muscle, we predict that the dissociation of MLCK from phosphorylated SMM is rate-limiting and that the rate of the phosphorylation step is faster than this dissociation rate. Also, association with SMM (11−46 s^{-1}) would be much faster than with pSMM (<0.1−0.2 s^{-1}). This suggests that the probability of MLCK interacting with unphosphorylated versus phosphorylated SMM is 55−460 times greater. This would avoid sequestering MLCK to unproductive interactions with previously phosphorylated SMM, potentially leading to faster rates of phosphorylation in muscle.

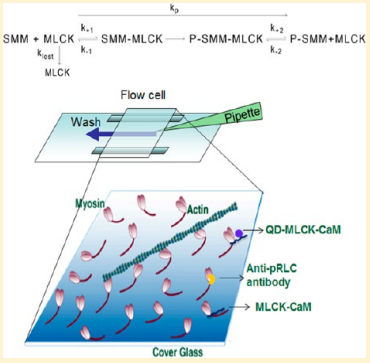

When activated by Ca^{2+}CaM, MLCK phosphorylates the SMM RLC at Ser19, which activates the actin−SMM ATPase leading to the cyclic interactions of SMM with actin required for smooth muscle contraction.[1−3] In smooth muscle, the level of MLCK is lower than the level of SMM, with an ∼1:20 MLCK:SMM molar ratio and an even lower activated MLCK:SMM molar ratio,[4−11] yet upon agonist activation of smooth muscle, the Ca^{2+}CaM−MLCK complex phosphorylates as much as 60% of the SMM in a relatively short (second) time.[12−15] Clearly, determining the kinetics of (i) SMM Ca^{2+}CaM−MLCK-activated phosphorylation, (ii) dissociation of MLCK from pSMM, and (iii) selective rebinding of MLCK to SMM is central to understanding the rate-limiting mechanisms of smooth muscle activation and the factors that may influence smooth muscle contractility.

MLCK is tightly associated with the contractile apparatus.[16−18] It contains both myosin and actin binding sites and has been shown to bind both actin and myosin in solution. The C-terminal telokin domain of MLCK binds to the SMM heavy chain at the junction between the two head domains and the tail domain. This places the MLCK catalytic core close to the two RLC subunits bound to each head domain. The stoichiometry of binding is one MLCK per molecule of SMM.[19]

Little is known about the kinetics of SMM phosphorylation by the Ca^{2+}CaM−MLCK complex. Sellers and co-workers have shown that SMM phosphorylation significantly decreases the affinity of MLCK for SMM in the absence of ATP (K_d from 0.8 to >100 μM).[20] However, it is unclear whether SMM phosphorylation decreases the MLCK−SMM association rate or increases the MLCK−SMM dissociation rate. The specific kinetic steps (association, phosphorylation, or dissociation) that limit the SMM phosphorylation rate have not been identified. Because the spectroscopic signals of association and dissociation that would be useful for standard transient kinetic studies in solution have not been developed, we have taken a nonspectroscopic approach. We have developed an *in vitro* model system in which smooth muscle proteins are attached to a coverslip surface in various configurations. This approach allows us (i) to control the constituents of the system, (ii) to

Received: July 25, 2013
Revised: October 16, 2013
Published: October 21, 2013

dx.doi.org/10.1021/bi401001x | *Biochemistry* 2013, 52, 8489−8500

measure the kinetics of SMM phosphorylation by MLCK and subsequent development of actin motion driven by surface-attached pSMM, and (iii) to observe directly the interactions of single MLCK molecules with single SMM molecules under similar conditions using TIRF microscopy.

We previously characterized MLCK and CaM−MLCK complexes that are copurified with SMM from chicken gizzard muscle.[18] With the CaM−MLCK−SMM complexes attached to a coverslip surface with SMM in the monomeric form, we showed that the MLCK was activated by Ca^{2+} to phosphorylate SMM, initiating actin filament sliding in an *in vitro* motility assay. The half-maximal actin sliding velocity was observed at pCa_{50} 6.1, similar to other *in vitro* and *in vivo* studies, suggesting that the CaM−MLCK complex was activated by Ca^{2+} in a physiological manner. We also showed that the MLCK reversibly interacted with the surface-attached SMM through its telokin domain, which is the known SMM-binding site on MLCK.

Here we use this *in vitro* system to correlate the rate of MLCK-induced SMM activation with the association and dissociation kinetics of single MLCK molecules interacting with surface-attached monomeric SMM (not filamentous). We found that the SMM phosphorylation rate of 1.17 s^{-1} $MLCK^{-1}$ is similar to the rate at which actin motility is activated and is comparable to the SMM−MLCK dissociation rate constant of 0.80 s^{-1} obtained from our single-molecule experiments. We also show that MLCK dissociates from SMM and pSMM at essentially the same rate, implying that the decrease in the affinity of SMM for MLCK upon SMM phosphorylation[20] results from a decrease in the pSMM−MLCK association rate. This suggests that in the MLCK−SMM kinetic cycle, dissociation of MLCK from pSMM is rate-limiting and that the rate of the intrinsic phosphorylation step is faster than the rate of this dissociation step. Using our measured dissociation rates and K_d values, and estimates of SMM concentrations in muscle, our measurements suggest that association with unphosphorylated SMM (11−46 s^{-1}) would be much faster than that with pSMM (0.1−0.2 s^{-1}) in the muscle environment.

MATERIALS AND METHODS

Reagents. Tris-glycine gels (4−20% acrylamide, 1.0 mm thick, 10 or 12 wells) were from GE Heath Sciences (Carlsbad, CA). D-(+)-Glucose, glucose oxidase, type VII BSA (low biotin), cow brain CaM, methylcellulose, nitrocellulose, and ATP were from Sigma-Aldrich (St. Louis, MO). Phalloidin was from Alexis Corp. (San Diego, CA). ATPγS was from Roche Diagnostics (Indianapolis, IN). EZ-link Sulfo-NHS-LC-LC-Biotin was from Thermo Scientific Inc. (Rockford, IL). Microscope coverslips (22 mm × 30 mm, 1.5 mm) were from Fisher Scientific Company LLC (Pittsburgh, PA). The Qdot 525 (λ = 525 nm) ITK Streptavidin Conjugate Kit was from Invitrogen (Eugene, OR) and contained ∼5−10 streptavidin conjugates per QD. DMCS-coated coverslips were prepared by being treated with the following reagents for 20 s each: 0.1 M H_2SO_4, H_2O, methanol, acetone, $CHCl_3$, and 2.5% DMCS in $CHCl_3$.[21]

Proteins. SMM was from frozen chicken gizzards as described previously[22] except that the last polymerization−depolymerization step was excluded. On the basis of sequences P10587, P02612, an dP02607-1, SMM is 530 kDa. SMM was thiophosphorylated in HMM buffer (10 mM MOPS, 50 mM NaCl, 0.2 mM EGTA, 2.0 mM $MgCl_2$, and 1 mM DTT) with 3.0 mM $CaCl_2$, 1 mM ATPγS, 10 μg/mL CaM, and 40 μg/mL MLCK at 25 °C for 0.5 h, followed by overnight incubation on ice.[23] The extent of thiophosphorylation was quantified by urea−polyacrylamide gel electrophoresis.[24]

MLCK was from frozen chicken gizzards as described previously[4] and was biotinylated by EZ-link Sulfo-NHS-LC-LC-Biotin (Thermo Scientific) according to the manufacturer's protocol, giving 2−5 biotins per MLCK. The kinase activity of biotinylated MLCK was 3.76 μmol mg^{-1} min^{-1}, comparable to that of MLCK without biotinylation (3.3 μmol mg^{-1} min^{-1}) using RLC as the substrate. Biotinylated MLCK and biotinylated MLCK with attached QDs were able to fully phosphorylate SMM RLC as measured in a urea gel assay[24] (data not shown). Studies of equilibrium binding of MLCK to SMM filaments (data not shown) showed that, relative to unmodified MLCK, biotinylated MLCK had a similar affinity in the presence of Ca^{2+}CaM but bound ∼4−5 times more weakly in the absence of Ca^{2+}CaM.[20] Binding affinities were as described previously,[20] except that the MLCK in the supernatant was measured by Western blot analysis.[18]

Actin (chicken pectoralis muscle[25]) for motility assays was incubated with equimolar TRITC-labeled phalloidin overnight[26] and stored on ice at 4 °C. Tropomyosin was obtained from chicken gizzards.[27] Protein concentrations were determined using the following extinction coefficients (1 mg/mL): 0.56 for SMM at 280 nm, 1.14 for MLCK at 280 nm, and 1.1 for F-actin at 280 nm.

***In Vitro* Motility Assays.** Motility assays were performed using a Nikon TE2000 epifluorescence microscope (Nikon TE-2000U, Technical Instruments, Burlingame, CA) with a Roper Cascade 512B camera (Princeton Instruments, Trenton, NJ). The procedures described here relate to Figures 1−3, with additional details provided in the figure legends. Myosin buffer consisted of 300 mM KCl, 25 mM imidazole, 1 mM EGTA, 4 mM $MgCl_2$, and 10 mM DTT (pH 7.0). Actin buffer consisted of 50 mM KCl, 50 mM imidazole, 2 mM EGTA, 8 mM $MgCl_2$, and 10 mM DTT (pH 7.0). Motility buffer consisted of 50 mM KCl, 50 mM imidazole (pH 7.0), 2 mM EGTA, 8 mM $MgCl_2$, 10 mM DTT, 2 mM ATP, 0.5% methylcellulose, and an oxygen scavenger system (0.1 mg/mL glucose oxidase, 0.018 mg/mL catalase, and 2.3 mg/mL glucose). Motility assays were performed as previously described[28] at 30 °C. SMM containing the copurified CaM−MLCK complex at the indicated concentrations in myosin buffer was applied to nitrocellulose-coated coverslips attached to glass slides using adhesive tape or plastic spacers (0.127 mm deep). This SMM preparation was described in our previous work.[18] The MLCK:SMM ratio could be reproduced from preparation to preparation at 1:73 ± 9, or 1 MLCK per 146 SMM heads. The actual amount of active MLCK present during the motility assay is estimated to be ∼1 MLCK per 2600 SMM heads, considering that only 15−30% (22% on average) of the total MLCK was present as the CaM−MLCK complex[18] and that ∼75% would be expected to wash off the coverslip prior to the assay, given the affinities measured in our prior work.[18] After 1 min, the coverslip was washed with 2 × 40 μL of myosin buffer. The nitrocellulose surface was blocked with 2 × 40 μL of 0.5% (w/v) BSA in actin buffer for 1 min, followed by 2 × 40 μL of 10 nM TRITC-labeled actin in actin buffer for 1 min, and two washes with 40 μL of actin buffer. Motility buffer (40 μL at the indicated Ca^{2+} concentrations) was loaded twice, and 30 s image sequences of one to five fields were recorded. Data from these one to five fields constituted one (n = 1) experiment.

Quantification of the Percent of SMM Phosphorylation by an On-Coverslip ELISA. We previously described our on-coverslip ELISA.[18] Standards of different percentages of SMM phosphorylation were mixtures of prephosphorylated SMM and SMM at different ratios at the same final concentrations used for Figure 1.

Direct Visualization of the QD−MLCK Molecule Dynamically Interacting with Surface-Attached SMM Using TIRF Imaging. *Experimental Section.* Flowcells were as described for motility assays. SMM (0.5 μg/mL) in myosin buffer was applied to untreated glass coverslips for 2 min at 25 °C. Using the four lowest values in Table 1 from Harris et al.,[29]

Table 1. Summary of Measured and Calculated Parameters for the *in Vitro* Model System

		experimental condition	
	data source	MLCK	Ca^{2+}CaM−MLCK with ATP
state of SMM		SMM	pSMM
initial phosphorylation rate (k_p^o)	Figure 1	−	0.045% s^{-1}
			1.17 SMM heads s^{-1} $MLCK^{-1}$
rate of loss of MLCK (k_{lost})	Figure 1	−	0.22% s^{-1}
average lifetime [τ_{on} (s)] and distributions (%)	Figure 7	1.09 ± 0.17 (36 ± 2%)	1.25 ± 0.06 (49 ± 2%)
		8.23 ± 0.48 (64 ± 2%)	12.39 ± 0.48 (51 ± 2%)
dissociation rate constants (k_{-1} for SMM and k_{+2} for pSMM) (s^{-1})	Figure 7	0.92 (36%)	0.80 (49%)
		0.12 (64%)	0.08 (51%)
association rate constants (k_{+1}) (estimated)	Figure 7 and K_d[a]	0.24 s^{-1} μM^{-1} for SMM	
		<0.01 s^{-1} μM^{-1} for pSMM	
association rate for Figure 1 (estimated)	Figures 1 and 7 and K_d	2.3−4.6 s^{-1} for SMM	

[a] K_d measured in solution with myosin filaments (3.8 μM SMM and >60 μM pSMM).

we estimate the average surface density to be 25 SMM molecules/μm^2, giving ∼200−230 nm between each SMM. Control surfaces without SMM were incubated for 2 min in 1% (w/v) BSA (Sigma; A3059) in myosin buffer. After 2 min, all surfaces were blocked with two 30 s washes of 1% BSA (w/v) in myosin buffer. Volumes of washes were typically 45−65 μL. The QD−MLCK molecule was prepared by mixing equal volumes of 1.2 nM QD (525 ITK, Invitrogen) in myosin buffer and 45 nM biotinylated MLCK in myosin buffer containing 2% (w/v) methylcellulose and incubating the mixture for 5 min at 25 °C, producing a 0.6 nM QD/22.5 nM MLCK mixture in 1% methylcellulose in myosin buffer. To prepare the CaM−MLCK complex, 1 μg/mL CaM, 2 mM $CaCl_2$, and 1 mM ATP were incubated for 1 h with biotinylated MLCK. The QD−MLCK molecule was applied to the coverslips and viewed immediately under TIRF conditions at 100× magnification using the same Nikon TE2000 epifluorescence microscope we used for the *in vitro* motility assays, but with a 488 nm excitation laser. Movies were captured with a Roper Cascade 512b instrument (Princeton Instruments, Trenton, NJ) at exposure rates of 87.9 ms/frame in SimplePCI. Typically, movies were captured for a little more than 1 min, and several movies were captured per slide. In several instances, flow cells were viewed continuously and intermittently for up to 30 min after preparation, but no obvious differences in the movies were detected. More than a dozen movies from at least three slides for the control, MLCK, and CaM−MLCK conditions were analyzed and quantified.

Data Analysis. The simple PCI files of image sequences were exported to TIFF format and viewed and analyzed in ImageJ 1.47b 64 bit and a demonstration version of Imaris version 7.5.1 (Bitplane, Zurich, Switzerland) on a OSX 10.7.5 Mac 3.4 GHz Intel core i7 computer. Imaris movies could be viewed as volumes (see Figure 6). Additional details of data analysis are given in Figure 1 of the Supporting Information.

QD Blinking Analysis. The Spots function in Imaris was used to analyze image sequences of control surfaces [without SMM (data not shown)]. Only nonspecifically bound QDs that remained attached to the surface for the duration of the movies were observed. These data were used to statistically analyze QD blinking behaviors so that we could identify blinks with confidence in the sequences of the interaction of the QD−MLCK molecule with SMM. Using the Spots function, we exported data to create pivot tables in Excel to determine the durations of 895 dark events (blinks). A statistical analysis using JMP (SAS, Cary, NC) showed that dark events that lasted more than six frames (0.53 s) were outliers (greater than 1.5 times the interquartile length of the distribution of all off times). From this, we defined a blink as a dark event that lasted six or fewer frames with a statistical confidence of greater than $p = 0.05$. Review of the data sets showed that a more stringent cutoff of $p = 0.01$ would not have changed the scoring of the data sets.

Criteria for a True Binding−Detachment Event. For image sequences of the QD−MLCK molecule interacting with surface-attached SMM, we set specific criteria that had to be satisfied before an event was included in the data set to determine the duration of attachment (see Figure 7). We excluded from analysis (i) QD−MLCK molecules that were bound for the duration of the image sequence, (ii) QD−MLCK molecules that were bound prior to the collection of movie data, (iii) transient binding or collision with the surface lasting only one frame, and (iv) QD−MLCK molecules that had traces in the exact same position after a dissociation event (or a QD dark event that lasted more than six frames to exclude blinks). We included QDs that clearly bound and detached (see Figure 6, up and down arrows) without returning to the same location, but dark events during this bound time had to last six or fewer frames (blink). QDs that were observed to bind and remained bound for the remainder of the image sequence were also counted.

In general, independent of the condition (QD, QD−MLCK, QD−MLCK−ATP, QD−MLCK−ATP−CaM, or QD−MLCK−CaM), there were occasionally as few as four QDs, rarely as many as 12 QDs, but most often nearly eight QDs bound to the surface in a manner suggesting nonspecific binding. These traces rarely had blink durations long enough to suggest dissociation events, but even in a case where the trace had statistically unnaturally long dark periods, the trace would be disregarded because we did not observe its association event. For Figure 7, a double-exponential fit to the survival curves was justified by comparing the sums of the mean-square residuals for single- and double-exponential fits, which gave F ratios of ∼50, which are in excess of the confidence levels necessary.[30] The equation for fitting was $y = A_1\, e(-t/\tau_{on1}) + A_2\, e(-t/\tau_{on2})$,

dx.doi.org/10.1021/bi401001x | *Biochemistry* 2013, 52, 8489−8500

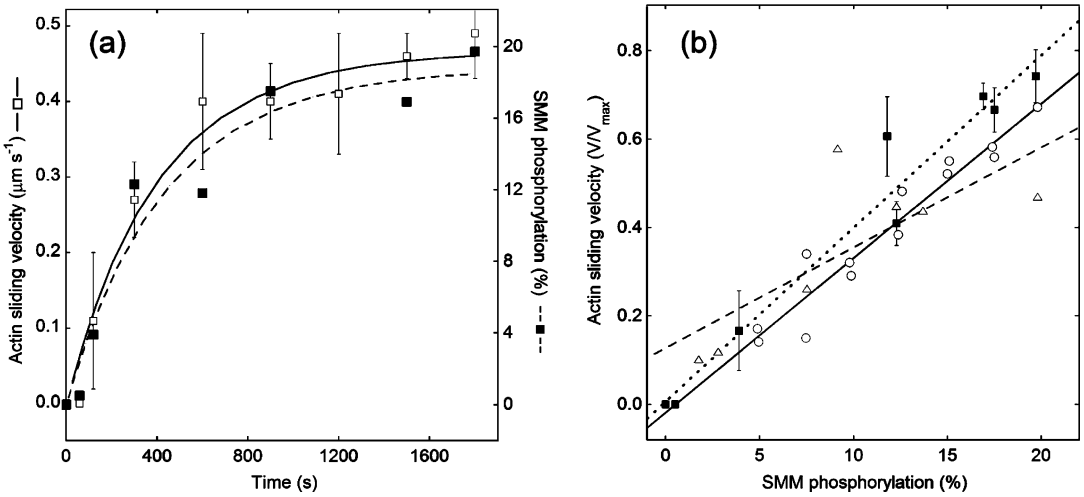

Figure 1. Kinetics of MLCK-induced mechanical activation and phosphorylation of the SMM RLC. (a) Nitrocellulose-coated coverslips were treated as follows (see In Vitro Motility Assays for further details): monomeric SMM (0.2 mg/mL) containing the copurified CaM−MLCK complex, BSA block, and 10 nM TRITC-actin filaments. Actin filament velocities measured at different times after incubation with motility buffer at pCa 4 (□) increase as SMM is phosphorylated by MLCK. Velocity data indicate the mean ± standard deviation from four SMM preparations and four independent measurements. For one experiment, after the motility assay was completed, each coverslip was washed and blocked, and an on-coverslip ELISA (see Materials and Methods) was performed to measure the pRLC level and the percent phosphorylation (■) by comparison to a standard curve.[18] Experiments with other SMM preparations with fewer time points showed a similar time course (not shown). (b) The velocity (V) and phosphorylation data from panel a along with a linear fit (■, dotted line; slope = 0.039; R^2 = 0.98) are plotted on the same graph with the data for known mixtures of SMM and pSMM (○, solid line; slope = 0.035; R^2 = 0.96[33]) and for SMM phosphorylated in solution representing a random mixture of unphosphorylated, one-head-phosphorylated- and two-head-phosphorylated species (△, dashed line; slope = 0.023; R^2 = 0.77[32]). Our maximal velocity (V_{max}) was 0.66 μm/s (measured after adding the exogenous CaM−MLCK complex), similar to the references quoted above (0.67 μm/s).

where $A_1 + A_2$ equals the total number of molecules analyzed in the data set and A_1 and A_2 are the respective fractional contributions for each exponential. All fitting was done by the least-squares method[31] using Kaleidagraph (Synergy Software), and τ_{on} values are reported with the standard error. Further details of the method are given in Figure 1 of the Supporting Information.

RESULTS AND DISCUSSION

Kinetics of Phosphorylation and Mechanical Activation of Surface-Attached Monomeric SMM by MLCK. We measured the kinetics of MLCK-induced phosphorylation of surface-attached monomeric SMM and the subsequent activation of actin filament sliding over the pSMM (Figure 1a). SMM containing the copurified CaM−MLCK complex[18] was attached to a nitrocellulose-coated coverslip in the absence of Ca^{2+} and ATP, and 10 nM fluorescent actin was added. No movement of actin was observed as expected because MLCK requires Ca^{2+} for enzymatic activity. Upon addition of motility buffer containing 100 μM free $CaCl_2$ (pCa 4) to activate the copurified CaM−MLCK complex and 2 mM ATP to provide a substrate for both SMM and MLCK, actin motility increased with time, reaching a maximal velocity of ~0.45 μm/s after 30 min [Figure 1a (□)]. This is lower than the maximal velocity (V_{max}) of 0.66 μm/s, which was observed for 100% prephosphorylated SMM, suggesting that the plateau in velocity in Figure 1a occurs before SMM is fully phosphorylated.

Using separate slides for each time point after the actin motility was recorded, we performed an on-coverslip ELISA to determine the level of RLC phosphorylation (percent of total) using our previously described method.[18] Figure 1a shows that following the addition of Ca^{2+}, the level of SMM phosphorylation increased with time, reaching a maximal level of phosphorylation of ~20% after 30 min [Figure 1a (■)].

Figure 1b shows the correlation between actin sliding velocities expressed as V/V_{max} and the percent phosphorylation from Figure 1a (■) with a linear fit (dotted line). Also plotted for reference are data and linear fits for randomly phosphorylated SMM [△, dashed line (taken from ref 32)] and mixtures of unphosphorylated and fully phosphorylated SMM [○, solid line (taken from ref 33)]. The three data sets are similar, showing a nearly linear relationship between V/V_{max} and percent phosphorylation within this range of phosphorylation. The similarity of the three data sets is evidenced by the slopes to linear fits (0.039, 0.034, and 0.023 for V/V_{max} per percent phosphorylation) and suggests three important points. First, our method for measuring the absolute levels of phosphorylation of surface-attached SMM by an ELISA gives the expected levels of phosphorylation at a given actin filament velocity, demonstrating that this is a robust way to measure phosphorylation kinetics in this *in vitro* system. Second, actin sliding velocities can be used to estimate phosphorylation rates within this range of phosphorylation. This is important because actin sliding velocities are much less labor intensive to measure than phosphorylation. Third, we cannot determine from the data in Figure 1 whether the MLCK is generating two-head-phosphorylated or a mixture of one-head- and two-head-phosphorylated SMM. It is likely that it is the latter, because it has been shown that MLCK phosphorylation kinetics in solution are consistent with a model in which phosphorylation of the two heads of SMM occurs randomly at equal rates.[34] Therefore, in Figure 1a, we expect that most pSMMs were phosphorylated on only one head because the level of maximal phosphorylation was only ~20%.

dx.doi.org/10.1021/bi401001x | *Biochemistry* 2013, 52, 8489−8500

The observation that the rate of SMM phosphorylation approaches zero at <100% phosphorylation (Figure 1a) suggests a loss of available MLCK over time, presumably through diffusion from the surface-attached SMM or by irreversibly binding to the coverslip surface. The former mechanism is supported by our observation that peak activation levels are >3-fold higher in the presence than in the absence of methylcellulose (Figure 2). In a motility assay, methylcellulose

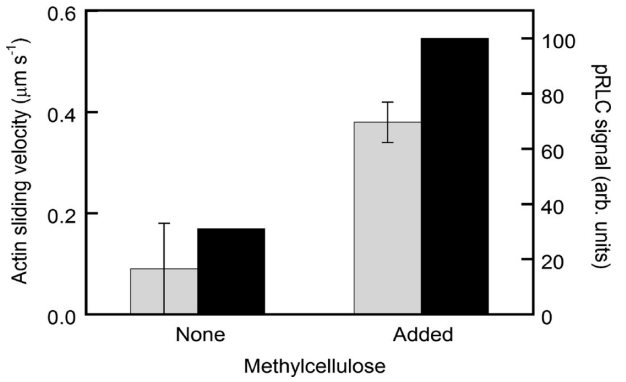

Figure 2. Effect of methylcellulose on MLCK-induced phosphorylation of SMM and on observed actin sliding velocities. Experimental conditions were as described in the legend of Figure 1 except that the incubation with motility buffer lasted for 10 min and motility buffer contained either no methylcellulose or 0.5% methylcellulose. The actin sliding velocity is shown by the gray bars, and the error bars for motility represent the standard deviation from four SMM preparations and five replicates. The pRLC signal is shown as black bars, and data are from a single determination.

holds actin filaments close to the surface, and it is possible that it does the same for MLCK. That is, it may decrease the probability that MLCK diffuses far from the SMM surface, effectively increasing the frequency of SMM−MLCK interactions. The low level of maximal activation does not result from contaminating phosphatase, because as shown below we observe similar subsaturating levels of phosphorylation when ATPγS is used instead of ATP. Thiophosphorylated SMM, unlike pSMM, is resistant to dephosphorylation by the phosphatase.

Scheme 1a accurately accounts for the data in Figure 1a (■). Phosphorylation of SMM occurs with a pseudo-first-order rate constant, k_p, that varies linearly with MLCK concentration. Because MLCK is depleted at a rate k_{lost}, k_p decreases with time and $k_p = k_p^\circ \times \exp(-k_{lost}t)$, where k_p° is the initial phosphorylation rate at the MLCK concentration at time zero. The dashed line in Figure 1a is a Matlab (Mathworks, Natick, MA) simulation based in Scheme 1a, which gives estimates for k_p° and k_{lost} of 0.045% s^{-1} (of SMM heads) and 0.22% s^{-1} [of MLCK (see Scheme 1b)], respectively. We estimate that at time zero there is one active MLCK per 2600 SMM heads (see Materials and Methods), so the initial activation rate, k_p°, is ∼1.17 heads s^{-1} $MLCK^{-1}$ (Table 1). The solid line in Figure 1a shows the simulation of the velocity data, assuming that the fractional velocity increases linearly with time (see Figure 1b), and the maximal velocity occurs at 19% phosphorylation. The resulting simulation of velocity data gave k_p° and k_{lost} values of 0.05% s^{-1} (of SMM heads) and 0.23% s^{-1} (of MLCK), respectively. Therefore, the simulations of phosphorylation and velocity gave essentially the same rates.

Scheme 1. Definition of Model and Kinetic Parameters[a]

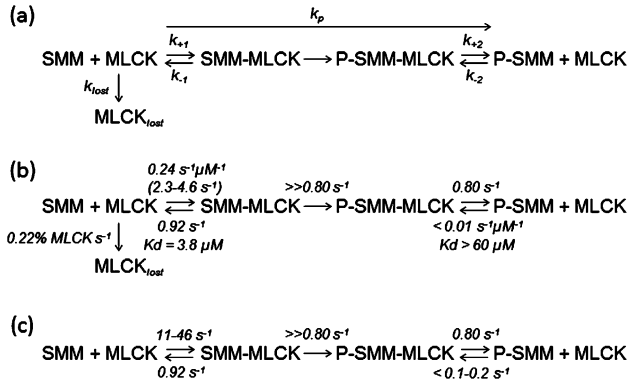

[a](a) Rate constants defined for the *in vitro* assay system and used for the Matlab fit to data in Figure 1a. (b) Rate constants measured and calculated along with rates (in parentheses) predicted using protein concentrations in the *in vitro* assay system. (c) Predicted rates for the same kinetic scheme as in panel b but under condtions found in smooth muscle. Values are either directly measured (Table 1) or calculated from estimates of protein concentrations in smooth muscle (see the text), using the rate and equilibrium constants from panel b.

Our estimated initial phosphorylation rate (k_p°) of ∼1.17 heads s^{-1} $MLCK^{-1}$ is similar to the rate of phosphorylation measured in solution under pseudo-first-order conditions for the monomeric form of SMM of 1.14 heads s^{-1} $MLCK^{-1}$.[34] This is also similar to our previous estimates[18] of MLCK activity in solution of 1.5 s^{-1} $MLCK^{-1}$. This implies that even with surface-attached SMM, the kinetics of phosphorylation by MLCK closely resemble the kinetics measured in solution studies.

Methylcellulose Enhances the Rate of MLCK-Induced Phosphorylation of SMM and MLCK-Induced Mechanical Activation of SMM To Move Actin Filaments. The experiments in Figure 1a were performed under standard motility assay conditions with methylcellulose in the buffer. Methylcellulose, an extended polymer, is used to limit the motion of the fluorescent actin to roughly two dimensions. In the absence of methylcellulose, we observed relatively slower actin sliding velocities and lower levels of SMM phosphorylation (Figure 2), suggesting that methylcellulose decreases k_{lost} (Scheme 1a) most likely by increasing the time the MLCK remains close to the surface-attached myosin. Also, methylcellulose may increase the rate of association of MLCK with SMM, if this step is rate-limiting under these conditions (see below). Alternatively, because actin is more confined to the surface in the presence of methylcellulose, the greater proximity of actin and SMM may allow MLCK to attach to both actin and SMM through the respective binding sites on opposite ends of the molecule. Transient attachment to moving actin filaments may facilitate phosphorylation of SMM. This would involve binding of MLCK to actin, which is then presented to SMM heads as the actin moves along, transporting the MLCK to the next SMM. The following section describes experiments designed to detect actin-mediated enhancement of motility and phosphorylation of SMM.

Effect of Actin on MLCK-Induced Mechanical Activation and SMM Phosphorylation. To examine the effects of actin movement on the rate of SMM activation (Figure 1), we performed a two-step experiment on coverslips coated with monomeric SMM containing copurified MLCK. In the first

dx.doi.org/10.1021/bi401001x | *Biochemistry* 2013, 52, 8489−8500

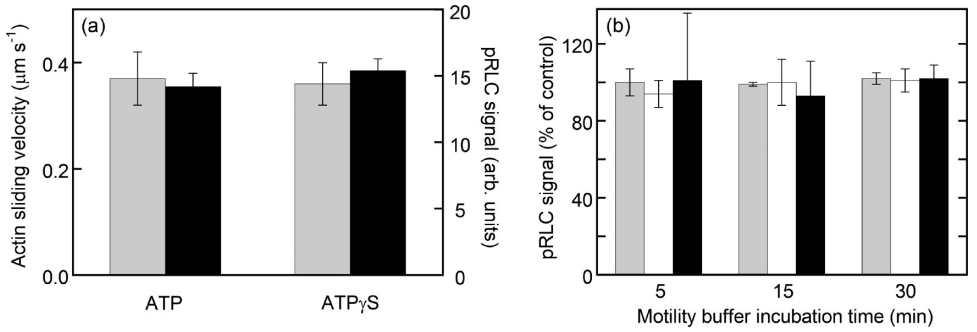

Figure 3. Effect of actin on phosphorylation of surface-attached SMM. (a) Effect of actin movement over surface-attached SMM. For step 1, nitrocellulose-coated coverslips were treated as follows (see In Vitro Motility Assays and Quantification of the Percent of SMM Phosphorylation by an On-Coverslip ELISA for further details): 0.1 mg/mL SMM containing the copurified CaM−MLCK complex, washed, blocked, 10 nM TRITC-actin, incubation in motility buffer containing either 2 mM ATP or ATPγS at pCa 4 for 15 min at room temperature (sliding velocity not recorded). For motility data shown as gray bars, step 2 was as follows: washed, reloaded 10 nM TRITC-actin, and motility assay performed (with 2 mM ATP) without added Ca^{2+}. The free Ca^{2+} concentration without added Ca^{2+} was estimated to be 1 nM. Data were collected immediately after the final motility buffer had been loaded. The velocity values indicate the mean ± the standard deviation. Data are from three SMM preparations and five independent measurements. There was no significant difference between the two treatments (t test; $p < 0.05$). For pRLC quantitation shown as black bars, step 2 was an ELISA procedure. Values indicate means ± the standard deviation from three measurements with no significant difference (t test; $p < 0.05$). (b) Effect of actin or actin-Tm on the SMM phosphorylation time course. Nitrocellulose-coated coverslips were treated as follows: 0.2 mg/mL SMM containing the copurified CaM−MLCK complex, washed, blocked, 10 nM actin (gray bars), 100 nM actin (white bars), or 100 nM actin with 50 nM Tm (black bars) in actin buffer or actin buffer alone (control), incubated with motility buffer with 2 mM ATP at pCa 4 for different times, followed by a wash, and ELISA for pRLC. Means ± the standard deviation are from three to seven repeats from two SMM preparations. Actin sliding velocities were ∼0.15−0.5 μm s^{-1} (similar to Figure 1).

step, to allow the SMM to be phosphorylated, the surface was incubated in standard motility assay buffer at pCa 4 in the presence of 10 nM TRITC-actin for 15 min but the actin sliding velocity was not recorded. The buffer contained either ATP or ATPγS. These nucleotides are used by MLCK to phosphorylate or thiophosphorylate SMM, respectively. On the other hand, SMM can use ATP but not ATPγS at an appreciable rate. Therefore, actin moves in the presence of ATP but not in the presence of ATPγS. In the second step, to determine the effects of the treatments from the first step, we washed out the motility assay buffers and re-added motility buffer (ATP) and TRITC-actin in the absence of added Ca^{2+} and immediately measured the actin sliding velocity. The gray bars in Figure 3a show that the actin sliding velocities for the ATP and ATPγS treatments were not significantly different. An identical set of coverslips were treated in the same manner for the first step, but the pRLC signal was measured by an ELISA in the second step. The black bars in Figure 3a show that the pRLC signals were very similar for the ATP and ATPγS treatments, consistent with the motility data. These data suggest that a similar amount of SMM phosphorylation and similar levels of actin motility occurred regardless of whether the actin was allowed to move over the surface-attached SMM during the phosphorylation reaction in step 1.

We next addressed whether actin was necessary for phosphorylation (Figure 1), and if increasing the actin concentration or substituting actin with actin-Tm enhanced the phosphorylation rate. Actin-Tm binds MLCK with an ∼4-fold higher affinity than actin alone.[20] The protocols for the experiments in Figure 3b were similar to those for Figure 3a except that in step 1 we included 0 nM (control), 10 nM (gray bars), or 100 nM actin (white bars) or 100 nM actin with 50 nM Tm (black bars). The incubation time in the presence of motility buffer containing Ca^{2+} and ATP was varied before measuring the pRLC signal by an ELISA on the coverslip. Data are plotted as the percent pRLC signal observed for the actin-treated coverslips relative to the pRLC signal obtained for coverslips treated with actin buffer alone (control). For all three incubation times, the pRLC signal obtained in the presence of actin was similar to that of the control. These data show that similar levels of SMM phosphorylation were attained over a 30 min time period at 0, 10, or 100 nM actin, and at 100 nM actin-Tm. In summary, under these conditions, (i) the presence of actin was not necessary to obtain phosphorylation kinetics similar to that shown in Figure 1 and (ii) adding higher actin concentrations or substituting actin with actin-Tm did not significantly affect phosphorylation kinetics. These results do not necessarily indicate or predict that actin−SMM interactions will not affect phosphorylation kinetics in muscle. Note that actin in Figure 1 is at a very low concentration, so that only a small fraction of the total surface-attached SMM is interacting with the actin at any point in time. This is true even at the higher actin concentration of 100 nM used above.

Visualization of Single QD−MLCK Molecules Statically Bound to SMM and to SMM in SMM−F-Actin Rigor Complexes Using TIRF Imaging. To visualize QD-labeled MLCK molecules bound to surface-attached monomeric SMM and to assess issues of nonspecific binding, we conducted the experiment in Figure 4a that shows a representative image of a DMCS-coated coverslip surface treated in sequence as follows (see Materials and Methods for details): (i) monomeric SMM, (ii) BSA block, (iii) biotinylated MLCK in the presence of CaM at pCa 4, (iv) wash, (v) QDs, (vi) wash, and (vii) motility buffer without ATP. The image shows that the surface was coated with a single QD (identified by blinking). The SMM and MLCK concentrations were purposefully high to increase the likelihood that a single QD was interacting simultaneously with more than one MLCK−SMM complex because of its multivalent streptavidin coating. Therefore, the lifetimes of the interactions were very long (>10 min). This allowed us to easily count a significant number of QDs in each field of view, without observing attachment or detachment events. Most QDs were bound specifically to the MLCK−SMM complex, because relatively few QDs were observed in the absence of either

dx.doi.org/10.1021/bi401001x | Biochemistry 2013, 52, 8489−8500

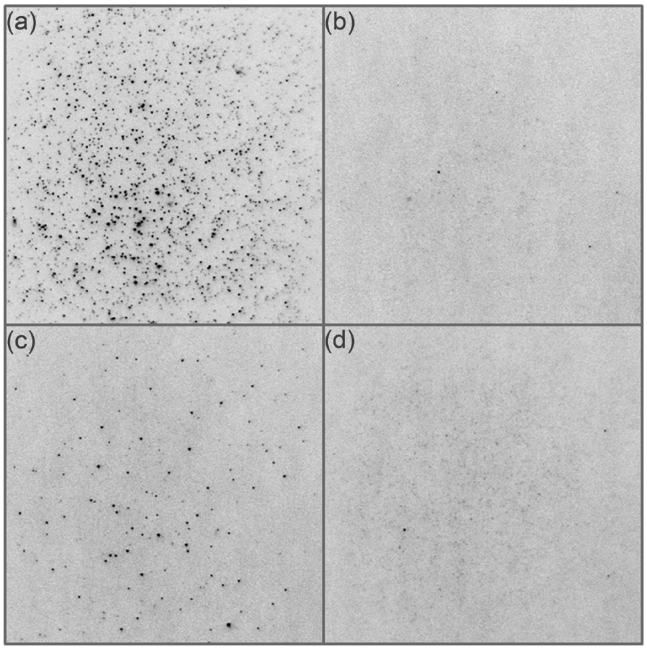

Figure 4. Visualization of single QD−MLCK molecules bound to SMM using TIRF microscopy. The instrumentation was as for motility assays except with a 488 nm excitation laser. Images are inverted so that QDs appear as dark spots. DMCS-coated coverslips were treated with the following reagents in order: (a) SMM (0.2 mg/mL, ∼0.4 μM) for 2 min in myosin buffer, blocked with 2% BSA for 2 h in actin buffer, a mixture of 0.2 μM biotinylated MLCK and 0.2 μM CaM at pCa 4 for 10 min, wash with actin buffer, 0.5 nM QDs in actin buffer for 1 min, wash, motility buffer without ATP and $CaCl_2$. (b) Same as panel a except that MLCK and CaM were omitted. (c) Blocked with 2% BSA for 2 h, followed by a mixture of 0.2 μM biotinylated MLCK and 0.2 μM CaM at pCa 4 for 10 min, wash, 0.5 nM QDs, wash, motility buffer without ATP and $CaCl_2$. (d) Blocked with 2% BSA for 2 h, 0.5 nM QDs, wash, motility buffer without ATP and $CaCl_2$. QD numbers in panels a−d were measured using the particle analysis tool in ImageJ and found to be 1090, 3, 91, and 6, respectively. The dimensions for all images are 54 μm × 54 μm.

biotinylated MLCK (Figure 4b) or SMM (Figure 4c), or to the blocked surface (Figure 4d). Note that under these conditions MLCK cannot phosphorylate the SMM on the surface (no ATP), and therefore, the QD−MLCK molecule is interacting with unphosphorylated SMM. In Figure 4, ∼10 times more QDs were observed if SMM and a BSA block were applied prior to adding MLCK, versus if only MLCK was applied to a BSA-blocked surface. This directly shows that the nonspecific binding of MLCK to a blocked surface is approximately $^1/_{10}$ of the binding observed for SMM.

To further demonstrate specific MLCK−SMM interactions, we also observed single QD−MLCK molecules bound to SMM that was in a SMM−F-actin rigor complex. We treated a DMCS-coated coverslip surface with the following sequence of incubations: TRITC-labeled F-actin, BSA block, a mixture of SMM and biotinylated MLCK with CaM at pCa 4, wash, QDs, wash, and motility buffer without ATP (note that motility buffer contains EGTA without added Ca^{2+}). Again, SMM and MLCK concentrations were high for the promotion of multivalent QD binding (see above). Using TIRF microscopy, both TRITC-actin (red) and QDs (green) were sequentially imaged in the same region of interest. Figure 5a is a representative combined image showing surface-attached actin (red) and QD-MLCK (green) with significant colocalization (yellow). Because MLCK is known to bind both SMM and actin, the QD−MLCK molecule in Figure 5a could be bound to either actin filaments, actin-bound SMM, or both. To distinguish between these possibilities, we repeated the experiments described above in the absence of SMM (Figure 5b) and observed relatively few QDs colocalized with F-actin (compare panels a and b of Figure 5). This suggests that the CaM−MLCK complex does not bind appreciably to actin filaments alone under these conditions. Note that we intentionally mixed MLCK with SMM in solution prior to a brief exposure to F-actin to minimize binding of MLCK to F-actin under this condition. We have observed that the QD−MLCK molecule binds F-actin under conditions that more effectively promote their binding (data not shown; manuscript in preparation)]. Because SMM was required to observe QD colocalization on actin, we conclude that MLCK first bound to monomeric SMM during the preincubation in solution, and the preformed MLCK−SMM complex then bound to surface-attached actin filaments through an acto-myosin rigor interaction.

Figure 5c shows a comparison of the number of QDs per micrometer of actin under various conditions. Conditions 1 and 4 correspond directly to those in panels a and b of Figure 5, respectively. For condition 1 with SMM, there was 0.75 QD per micrometer of actin, whereas under condition 4 in the absence of SMM, there was only 0.03. In the absence of MLCK (condition 5), QDs did not bind to the surface, suggesting that the QDs bound specifically to MLCK.

Because the QD−MLCK−SMM complexes in Figure 5a were bound to surface-attached actin in a rigor state (no ATP), addition of ATP to the final motility buffer should dissociate SMM (with the bound QD−MLCK molecule) from actin if the MLCK−SMM complex were specifically bound to actin but not if it were bound to the surface. Upon addition of MgATP, most QDs dissociated from the surface. The addition of 2 and 20 μM MgATP (conditions 2 and 3, respectively) decreased the number of QDs per micrometer of actin filament in a concentration-dependent manner. This effect is quantified in Figure 5c. Figure 5c includes cartoons depicting our interpretation of the results described above. The data in Figure 5 suggest that the CaM−MLCK complex can bind tightly to monomeric SMM in solution, and that the CaM−MLCK−SMM complex can bind to F-actin through the actin-binding site on myosin. Importantly, as in Figure 4, the data in Figure 5 again demonstrate weak nonspecific binding to the surface.

Direct Visualization of the QD−MLCK Molecule Dynamically Interacting with Surface-Attached SMM Using TIRF Imaging. Having addressed nonspecific binding issues (Figures 4 and 5), we moved on to measure dynamic MLCK−SMM interactions to understand which processes may limit the rate of the phosphorylation reaction from Figure 1a. Our first objective was to quantify the lifetimes of QD−MLCK−SMM interactions (τ_{on}) to determine the rate of dissociation of MLCK from SMM [k_{-1} (Scheme 1a)] or from pSMM [k_{+2} (Scheme 1a)]. The data in Figures 6 and 7 were obtained under conditions similar to those used for Figure 1 except that we used a much lower density of SMM (0.5 μg/mL), resulting in a surface density of ∼25 SMM molecules/μm^2,[29] corresponding to ∼200−230 nm spacing between each SMM assuming two-dimensional hexagonal packing. This low density was used to increase the probability that the QD−MLCK molecule bound to only one SMM at a time, while still

dx.doi.org/10.1021/bi401001x | *Biochemistry* 2013, 52, 8489−8500

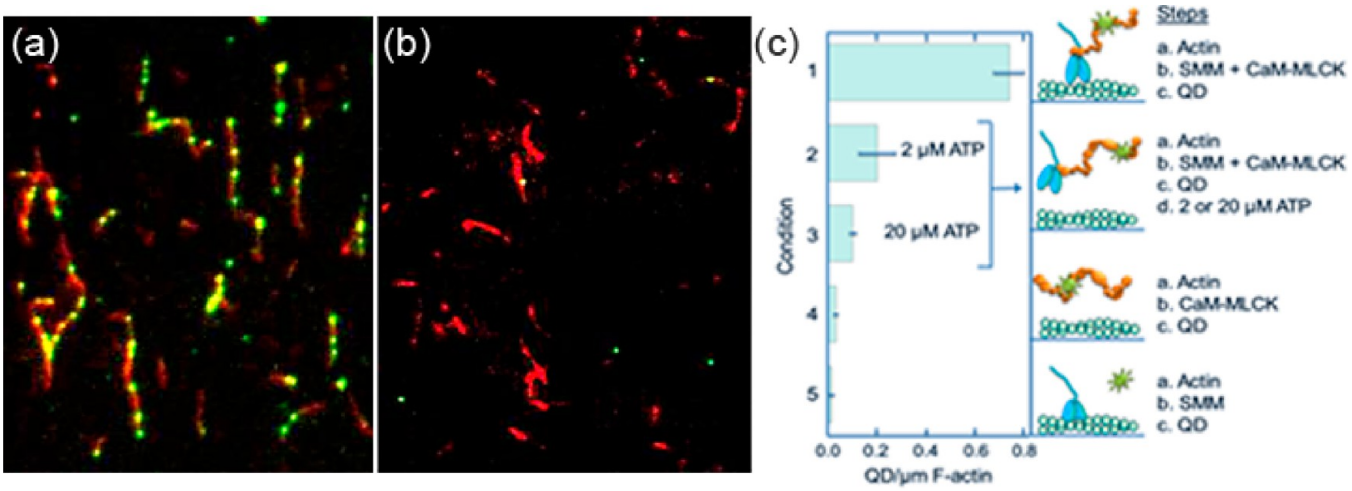

Figure 5. TIRF imaging demonstrating CaM−MLCK−SMM complexes bound to F-actin. (a) A DMCS-coated coverslip surface was treated in sequence as follows: 125 nM TRITC-actin for 20 min in actin buffer, block for 2 h with 2% BSA in actin buffer, a mixture of 0.4 μM (0.2 mg/mL) SMM, 0.2 μM biotinylated MLCK, and 0.2 μM CaM at pCa 4 for 2 min, wash, 0.5 nM QDs for 1 min, wash, motility buffer without ATP. The cube on the microscope was switched to record both TRITC-actin (red) and QD (green) images in the same observing areas. Note the strong colocalization of actin and the QD−MLCK molecule. (b) Representative image from an experiment identical to that used for panel a except there was no SMM in the mixture of biotinylated MLCK and CaM. Note the lack of significant colocalization of actin and the QD−MLCK molecule. (c) Number of QDs per micrometer of actin determined for conditions 1−5. Values are means of data from three fields ± the standard error of the mean (error bars). The total numbers of QDs counted for conditions 1−5 were 547, 117, 48, 13, and 9, respectively. The coverslip treatment sequences are summarized at the right, and the details are the same as those described for panels a and b. Under condition 4, the SMM step was omitted, and under condition 5, the MLCK and CaM were omitted and no ATP was in the motility buffer. The corresponding cartoons depict our interpretation of the results. Actin is colored green and attached to the coverslip surface (blue line). SMM blue, MLCK orange, and QD green.

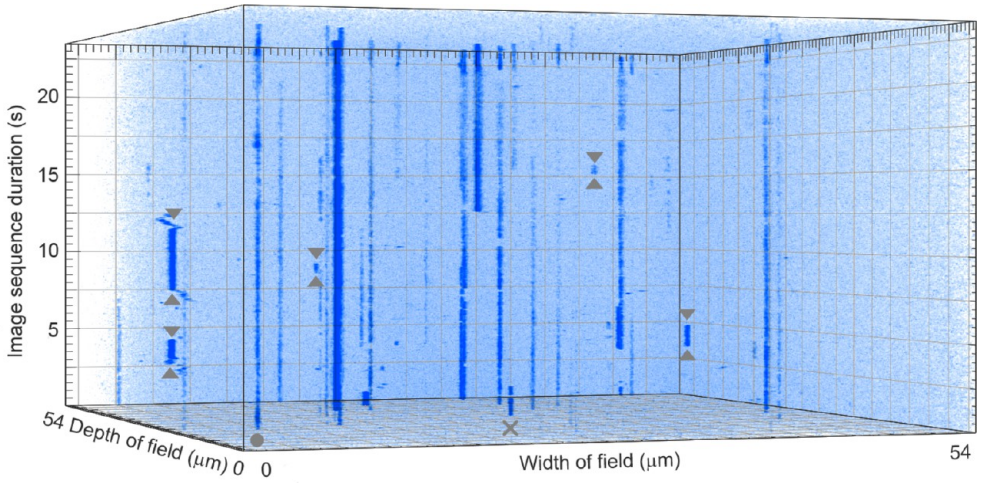

Figure 6. Three-dimensional kymograph of a representative image sequence for the interaction of the QD−MLCK molecule with surface-attached SMM using TIRF. The field of view is 512 pixels × 512 pixels (54 μm × 54 μm). The total duration is 24.35 s or 277 frames. Vertical blue lines are kymographs of QD−MLCK molecules. For further details of the experiment, see Materials and Methods, and for further details of the analysis method, see Figure 1 of the Supporting Information. A few but not all instances of binding−detachment events that meet the criteria described in Materials and Methods are bracketed with up and down arrows. Examples of data not meeting the criteria are QD−MLCK binding that began before the initiation of the movie (X) and a QD−MLCK molecule showing no binding event or dissociation event (filled circle).

allowing for a measurable number of events. Using QD (with streptavidin included, 20 nm in diameter) and predicted MLCK dimensions,[35] we estimated that a single QD−MLCK molecule could not simultaneously bind to more than one SMM if they were more than 80 nm apart. After blocking had been conducted, a mixture of 22.5 nM biotinylated MLCK and 0.6 nM QD in motility buffer (1% methylcellulose) was applied to the surface, and image sequences were recorded.

Figure 6 is a three-dimensional kymograph of a QD−MLCK molecule interacting dynamically with a SMM-coated surface, showing QDs binding to and detaching from the surface over time (a blue line is a single kymograph of one QD). The blinking of bound QDs appears as rapid fluctuations in the intensity of the blue lines (not indicated in the figure). In contrast, a blue line starting and then ending indicates a QD has bound to and detached from the surface (see up and down arrows bracketing binding−detachment events). We excluded binding−detachment events that re-occurred at the same location, with the assumption that they may represent tethered molecules appearing in and out of the TIRF field. We assumed that MLCK had to detach from one SMM before it could reach another SMM and that the probability of any one SMM being

dx.doi.org/10.1021/bi401001x | *Biochemistry* 2013, 52, 8489−8500

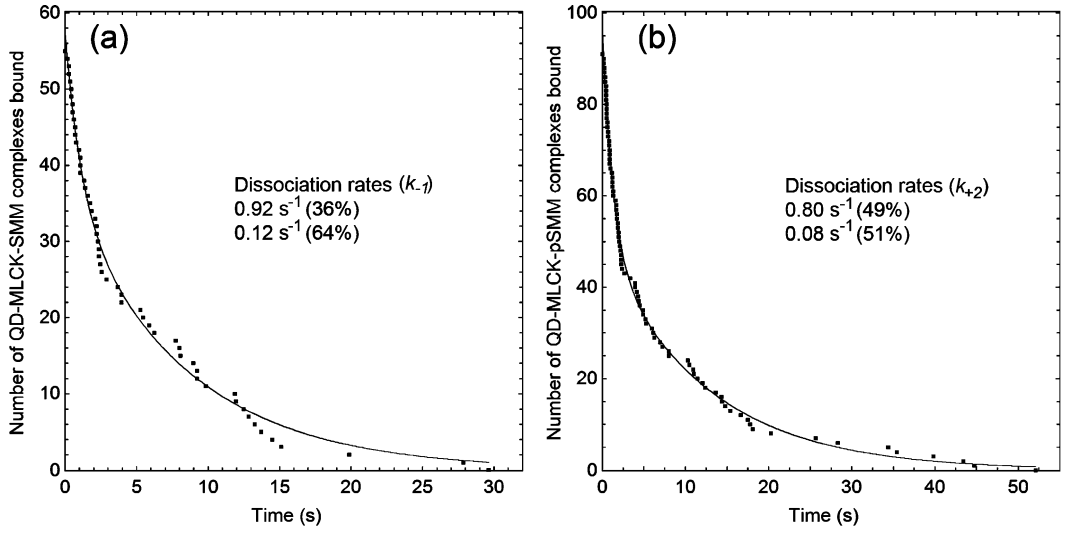

Figure 7. Determination of the rate of dissociation of the QD−MLCK molecule from surface-attached SMM. Data taken from image sequences similar to those described in the legend of Figure 6 (also see Figure 1 of the Supporting Information) are plotted as survival curves. The durations of all binding events that meet the criteria (see Materials and Methods) are plotted on the *X*-axis, and plotted on the *Y*-axis is the number of surviving QD−MLCK−SMM complexes or the number remaining bound at that time from the data set. Conditions are (a) the absence and (b) the presence of ATP and Ca^{2+}CaM in which the SMM on the surface is unphosphorylated and phosphorylated, respectively. For panel a, event durations from 14 image sequences were compiled (~350 s), or for panel b, event durations from 20 image sequences were compiled (~500 s). Double-exponential fits to the data are shown as solid lines. Dissociation rates and fractional contributions are summarized in the legends.

visited more than once during a given experiment was low. Binding−detachment events were included in the data sets for Figure 7 only if they met the criteria described in Materials and Methods and in Figure 1 of the Supporting Information. Nonspecifically bound QDs are also seen in Figure 6, an example of which is indicated with a filled circle. These QDs remain bound for the duration of the image sequence. In Figure 6, there are approximately six continuously bound traces, five unobserved association event traces, and 12 binding−detachment traces (not all indicated in the figure for the sake of clarity). This was a typical ratio.

The durations of QD−MLCK−SMM binding events that met our criteria were plotted as survival curves for experiments performed both without (Figure 7a) and with (Figure 7b) ATP and Ca^{2+}CaM. Under the latter condition, we estimated that SMM was fully phosphorylated by the time measurements were made (direct measurement of the phosphorylation was not possible at this low SMM density). Survival curves are best typically used to plot time until death or some other "time to event outcome variable" for a cohort of patients. However, this type of analysis can be used with any outcome variable that has a well-defined end point that can happen only once per subject or observation. In our case, the subject is an observable QD−MLCK−SMM complex and "survival" refers to the time that each QD−MLCK−SMM complex "survives" or the duration of the QD−MLCK−SMM binding event. To generate the survival curve, the measured duration of all the events is plotted on the *X*-axis and plotted on the *Y*-axis is the number of surviving QD−MLCK−SMM complexes in the data set at that time. The point at time zero represents the total number of events measured because all of those events are surviving at time zero.

We assume our events satisfy the ergodic theorem,[36] meaning that we observe the behaviors of individual molecules for a sufficient time so that when the event data are combined they approximate all the states that are seen in an infinite population in an instant in time. Therefore, the survival curves can be considered the equivalent of a first-order decay in solution kinetics and can therefore be fit to an exponential function.[37] This fit yields the average lifetime of the binding events or duration (τ_{on}) in seconds, and the rate of detachment of the QD−MLCK molecule from SMM equals $1/\tau_{on}$ in inverse seconds. In our case, double-exponential fits were justified as described in Materials and Methods. For SMM [absence of Ca^{2+}CaM and ATP (Figure 7a)], the fit gave τ_{on} values of 1.09 ± 0.17 s (36%) and 8.23 ± 0.48 s (64%), respectively. In the presence of Ca^{2+}CaM and ATP (Figure 7b), the fit gave a very similar result, τ_{on} values of 1.25 ± 0.06 s (49%) and 12.39 ± 0.48 s (51%), respectively.

The shorter lifetimes give MLCK dissociation rate constants ($1/\tau_{on}$) of 0.92 SMM s^{-1} (from SMM or k_{-1}) and 0.80 SMM s^{-1} (from pSMM or k_{+2}) (Table 1), indicating that MLCK dissociates from SMM and pSMM at similar rates. The value for dissociation of MLCK from pSMM of 0.80 SMM s^{-1} is similar to the rate constant k_p^o of 1.17 SMM heads s^{-1} MLCK^{-1} estimated from Figure 1, suggesting the dissociation of MLCK from pSMM is the step that is limiting the rate of phosphorylation seen in Figure 1. The longer lifetimes (slower dissociation rates) from the double-exponential fits were much slower than k_p^o, suggesting a process that is not in effect in Figure 1a. Most likely, these slower dissociation rates are due to multivalent interactions of the QD−MLCK molecule with more than one closely spaced SMM molecule (mentioned above), a situation that is possible even at the very low SMM densities used in the experiments.

Estimation of the MLCK−SMM Association Rate Constants. It is known from equilibrium binding experiments[20] that the binding of MLCK to pSMM is weaker than that to SMM. Thus, our data suggest that the association rate constant for binding of MLCK to pSMM is slower than for binding of MLCK to SMM. To directly measure the MLCK−SMM association rate constant at a single-molecule level, a QD−MLCK molecule must be tracked to record the time it spends diffusing prior to binding to a SMM molecule. Unfortunately, the diffusion of a single QD is impossible to

dx.doi.org/10.1021/bi401001x | *Biochemistry* 2013, 52, 8489−8500

track. Thus, we estimate the MLCK−SMM association rate constant, k_{+1}, to equal k_{-1}/K_d, where K_d is the dissociation constant (which we measured as ∼3.8 μM in the presence of Ca^{2+}CaM for SMM filaments using the same method used by Sellers et al.[20]) and k_{-1} is the MLCK−SMM dissociation rate constant (which we estimate above to be 0.92 s^{-1}). Thus, k_{+1} = 0.92 s^{-1}/3.8 μM = 0.24 s^{-1} μM^{-1} (Scheme 1b). For pSMM, the corresponding K_d (with Ca^{2+}CaM) is difficult to measure because it is very weak. Nevertheless, our measurements using the same method described above (ref 20 and data not shown) give a lower limit for K_d of 60 μM. The association rate constant, k_{-2}, for pSMM is estimated by k_{+2}/K_d = 0.80 s^{-1}/60 μM, which is <0.01 s^{-1} μM^{-1} (Scheme 1b). Therefore, MLCK associates at least 24 fold faster (0.24/0.01) with SMM than with pSMM. The C-terminal end of the telokin domain of MLCK is important for SMM binding.[20] This region is very negatively charged and likely is attracted to the positively charged region at the SMM head−tail junction where it is known to bind. Therefore, it makes molecular sense that adding negative charges on the pRLCs near this junction would slow of the rate of association.

In Figure 1, there are approximately 1150 SMM/μm^2.[29] If MLCK molecules diffuse within a methylcellulose-capped depth of 100−200 nm, there are 575−1150 SMM per 10^{-16} L, or roughly 9.5−19 μM SMM, giving an observed association rate of (0.24 s^{-1} μM^{-1})(9.5−19 μM) = 2.3−4.6 s^{-1} (Scheme 1b). This indicates that the rate at which MLCK phosphorylates SMM under the conditions described in the legend of Figure 1 is likely limited by the rate of both SMM−MLCK dissociation and association steps, because both rates are similar to the initial rate of phosphorylation ($k_p°$) of 1.17 s^{-1} $MLCK^{-1}$ determined from data in Figure 1.

Implications for the Kinetics of Interactions of MLCK with SMM in Smooth Muscle. Scheme 1c is a summary of the observed rates in the MLCK−SMM kinetic cycle that we estimate to be in effect in smooth muscle based upon our measurements in the *in vitro* system. The calculated observed association rate (2.3−4.6 s^{-1}) depends on the SMM concentration used on the coverslip, which is approximately 5−10-fold lower than that found in smooth muscle.[5−7] Therefore, in muscle it is likely that the association rate would be 5−10-fold faster or 11−46 s^{-1}. These values are much faster than the rate of dissociation from pSMM measured here (k_{+2} = 0.80 s^{-1}). Therefore, if the dissociation rate in muscle is similar to what we measure in the *in vitro* system, then dissociation of MLCK from pSMM would be the rate-limiting step in the SMM phosphorylation kinetic cycle in muscle.

To use the information listed above to predict rates in muscle, we estimate that the concentration of pSMM is 20% of that of SMM at the initiation of contraction (9.5−19 μM). This gives a rate of association of MLCK with pSMM in muscle of less than (9.5−19 μM)(0.01 s^{-1} μM^{-1}) or less than 0.1−0.2 s^{-1} (Scheme 1c). This rate is 55−460 times slower than the rate of association with SMM (11−46 s^{-1}) expected in the muscle. Therefore, an MLCK molecule that detaches from pSMM is ∼55−460 times more likely to attach to a SMM than to a pSMM. This may be a mechanism for increasing phosphorylation rates in the muscle, by kinetically partitioning the MLCK molecules, which are in limiting amounts and probably restricted in space, to productive interactions with only those SMM that have not yet been phosphorylated.

If the kinetics measured here accurately reflect what is happening in smooth muscle, we expect that the initial rate of SMM phosphorylation *in situ* would be similar in magnitude to our proposed rate-limiting step of dissociation of the Ca^{2+}CaM−MLCK complex from pSMM of 0.80 s^{-1}. Injeti et al.[7] measured this rate along with measurements of *in situ* MLCK and SMM concentrations in molar units and found the *in situ* MLCK activity in adult sheep carotid arteries to be 1.4 heads s^{-1} $MLCK^{-1}$, very similar to our value of 0.80 s^{-1}. In other studies in which the MLCK:SMM ratio was not measured, the corresponding value can be calculated by estimating the MLCK:SMM ratio to be 1 MLCK to 40 unphosphorylated heads (20 SMM). For the trachealis muscle, values range from ∼4.4−15 heads s^{-1} $MLCK^{-1}$ for neural stimulation[12,13] to ∼0.27−0.46 heads s^{-1} $MLCK^{-1}$ for stimulation with a cholinergic agonist.[14,15] These values range across the value of our proposed rate-limiting step. Therefore, the kinetics measured in this *in vitro* system are consistent with the measured kinetics of SMM phosphorylation in smooth muscle.

In summary, we have developed an *in vitro* assay to measure the rate of surface-attached SMM phosphorylation and the rate of mechanical activation of SMM to move actin filaments. A major advantage of our system is that single-molecule measurements, such as single-molecule dissociation rates, can also be made under very similar conditions. Because concentrations of the constituents in the assay are known with reasonable certainty, association rate constants can be estimated, as well. Comparisons and/or correlations of different kinetic measurements can be applied to a simple kinetic model to make predictions about the rate-limiting steps in the kinetic cycle of MLCK−SMM interactions in muscle. We are the first to show that SMM phosphorylation has an insignificant effect on MLCK−SMM dissociation rates, meaning that the weakening of the SMM:MLCK equilibrium binding affinity by phosphorylation is due to a decrease in the association rate constant. By comparing the rate of phosphorylation of SMM to the rate of dissociation of MLCK from pSMM and using these values to predict association rates in muscle, we conclude that dissociation of MLCK from pSMM would be the rate-limiting step in the SMM phosphorylation kinetic cycle in muscle. We believe that this assay system has potential for studying effectors of SMM activation kinetics such as actin, phosphatase, small molecules, MLCK mutations, and filamentous SMM.

■ ASSOCIATED CONTENT

Ⓢ Supporting Information

Additional details about the method used to determine the rate of dissociation of the QD−MLCK molecule from surface-attached SMM and pSMM relating to Figures 6 and 7 (Figure 1). This material is available free of charge via the Internet at http://pubs.acs.org.

■ AUTHOR INFORMATION

Corresponding Author

*E-mail: jebaker@unr.edu. Phone: (775) 784-4103.

Funding

This work was supported by National Heart, Lung and Blood Institute Grant 5R01HL110214 (to C.R.C., K.C.F., and J.E.B.), National Institutes of Health P20 Grant RR018751-07 (to J.E.B.), and Canadian Institutes of Health Research Grant MOP-111262 (to M.P.W.). M.P.W. is an Alberta Innovates-Health Solutions Scientist and Canada Research Chair (Tier 1) in Vascular Smooth Muscle Research.

Notes

The authors declare no competing financial interest.

■ ABBREVIATIONS

SMM, smooth muscle myosin purified from chicken gizzards (unphosphorylated unless indicated otherwise); pSMM, phosphorylated SMM; CaM, calmodulin; Ca^{2+}CaM, clamodulin with Ca^{2+} bound; MLCK, smooth muscle myosin light chain kinase; RLC, smooth muscle myosin regulatory light chain; pRLC, phosphorylated smooth muscle myosin regulatory light chain; TRITC, tetramethylrhodamine isothiocyanate; TRITC-actin, actin labeled with TRITC-phalloidin; Tm, smooth muscle tropomyosin; DMCS, dimethylchlorosilane; TIRF, total internal reflection fluorescence; ELISA, enzyme-linked immunosorbent assay; QD, streptavidin-coated quantum dot; ATPγS, adenosine 5′-[γ-thio]triphosphate.

■ REFERENCES

(1) Sobieszek, A. (1977) Ca-linked phosphorylation of a light chain of vertebrate smooth-muscle myosin. *Eur. J. Biochem. 73*, 477−483.

(2) Adelstein, R. S., and Eisenberg, E. (1980) Regulation and kinetics of the actin-myosin-ATP interaction. *Annu. Rev. Biochem. 49*, 921−956.

(3) Hartshorne, D. J., and Siemankowski, R. F. (1981) Regulation of smooth muscle actomyosin. *Annu. Rev. Physiol. 43*, 519−530.

(4) Walsh, M. P., Hinkins, S., Dabrowska, R., and Hartshorne, D. J. (1983) Smooth muscle myosin light chain kinase. *Methods Enzymol. 99*, 279−288.

(5) Dabrowska, R., Hinkins, S., Walsh, M. P., and Hartshorne, D. J. (1982) The binding of smooth muscle myosin light chain kinase to actin. *Biochem. Biophys. Res. Commun. 107*, 1524−1531.

(6) Ruegg, J. C. (1988) Calcium in Muscle Activation: A Comparative Approch. In *Zoophysiology and Ecology* (Burggren, W., Ishii, S., Johansen, K., Langer, H., Neuweiler, G., Randall, D. J., and Farner, D. S., Eds.) pp 201−235, Springer-Verlag, Berlin.

(7) Injeti, E. R., Sandoval, R. J., Williams, J. M., Smolensky, A. V., Ford, L. E., and Pearce, W. J. (2008) Maximal stimulation-induced in situ myosin light chain kinase activity is upregulated in fetal compared with adult ovine carotid arteries. *Am. J. Physiol. 295*, H2289−H2298.

(8) Isotani, E., Zhi, G., Lau, K. S., Huang, J., Mizuno, Y., Persechini, A., Geguchadze, R., Kamm, K. E., and Stull, J. T. (2004) Real-time evaluation of myosin light chain kinase activation in smooth muscle tissues from a transgenic calmodulin-biosensor mouse. *Proc. Natl. Acad. Sci. U.S.A. 101*, 6279−6284.

(9) Geguchadze, R., Zhi, G., Lau, K. S., Isotani, E., Persechini, A., Kamm, K. E., and Stull, J. T. (2004) Quantitative measurements of Ca^{2+}/calmodulin binding and activation of myosin light chain kinase in cells. *FEBS Lett. 557*, 121−124.

(10) Hong, F., Haldeman, B. D., Jackson, D., Carter, M., Baker, J. E., and Cremo, C. R. (2011) Biochemistry of smooth muscle myosin light chain kinase. *Arch. Biochem. Biophys. 510*, 135−146.

(11) Tansey, M. G., Luby-Phelps, K., Kamm, K. E., and Stull, J. T. (1994) Ca^{2+}-dependent phosphorylation of myosin light chain kinase decreases the Ca^{2+} sensitivity of light chain phosphorylation within smooth muscle cells. *J. Biol. Chem. 269*, 9912−9920.

(12) Kamm, K. E., and Stull, J. T. (1985) Myosin phosphorylation, force, and maximal shortening velocity in neurally stimulated tracheal smooth muscle. *Am. J. Physiol. 249*, C238−C247.

(13) Miller-Hance, W. C., Miller, J. R., Wells, J. N., Stull, J. T., and Kamm, K. E. (1988) Biochemical events associated with activation of smooth muscle contraction. *J. Biol. Chem. 263*, 13979−13982.

(14) de Lanerolle, P., and Stull, J. T. (1980) Myosin phosphorylation during contraction and relaxation of tracheal smooth muscle. *J. Biol. Chem. 255*, 9993−10000.

(15) Silver, P. J., and Stull, J. T. (1984) Phosphorylation of myosin light chain and phosphorylase in tracheal smooth muscle in response to KCl and carbachol. *Mol. Pharmacol. 25*, 267−274.

(16) Adelstein, R. S., and Klee, C. B. (1982) Purification of smooth muscle myosin light-chain kinase. *Methods Enzymol. 85* (Part B), 298−308.

(17) Wirth, A., Schroeter, M., Kock-Hauser, C., Manser, E., Chalovich, J. M., De Lanerolle, P., and Pfitzer, G. (2003) Inhibition of contraction and myosin light chain phosphorylation in guinea-pig smooth muscle by p21-activated kinase 1. *J. Physiol. 549*, 489−500.

(18) Hong, F., Haldeman, B. D., John, O. A., Brewer, P. D., Wu, Y. Y., Ni, S. W., Wilson, D. P., Walsh, M. P., Baker, J. E., and Cremo, C. R. (2009) Characterization of tightly-associated smooth muscle myosin-light chain kinase-calmodulin complexes. *J. Mol. Biol. 390*, 879−892.

(19) Silver, D. L., Vorotnikov, A. V., Watterson, D. M., Shirinsky, V. P., and Sellers, J. R. (1997) Sites of interaction between kinase-related protein and smooth muscle myosin. *J. Biol. Chem. 272*, 25353−25359.

(20) Sellers, J. R., and Pato, M. D. (1984) The binding of smooth muscle myosin light chain kinase and phosphatases to actin and myosin. *J. Biol. Chem. 259*, 7740−7746.

(21) Sundberg, M., Rosengren, J. P., Bunk, R., Lindahl, J., Nicholls, I. A., Tågerud, S., Omling, P., Montelius, L., and Månsson, A. (2003) Silanized surfaces for in vitro studies of actomyosin function and nanotechnology applications. *Anal. Biochem. 323*, 127−138.

(22) Ikebe, M., and Hartshorne, D. J. (1985) Effects of Ca^{2+} on the conformation and enzymatic activity of smooth muscle myosin. *J. Biol. Chem. 260*, 13146−13153.

(23) Ellison, P. A., Sellers, J. R., and Cremo, C. R. (2000) Kinetics of smooth muscle heavy meromyosin with one thiophosphorylated head. *J. Biol. Chem. 275*, 15142−15151.

(24) Wahlstrom, J. L., Randall, M. A., Jr., Lawson, J. D., Lyons, D. E., Siems, W. F., Crouch, G. J., Barr, R., Facemyer, K. C., and Cremo, C. R. (2003) Structural model of the regulatory domain of smooth muscle heavy meromyosin. *J. Biol. Chem. 278*, 5123−5131.

(25) Spudich, J. A., and Watt, S. (1971) The regulation of rabbit skeletal muscle contraction. I. Biochemical studies of the interaction of the tropomyosin-troponin complex with actin and the proteolytic fragments of myosin. *J. Biol. Chem. 246*, 4866−4871.

(26) Warshaw, D. M., Desrosiers, J. M., Work, S. S., and Trybus, K. M. (1990) Smooth muscle myosin cross-bridge interactions modulate actin filament sliding velocity in vitro. *J. Cell Biol. 111*, 453−463.

(27) Smillie, L. B. (1982) Preparation and identification of α- and β-tropomyosins. *Methods Enzymol. 85* (Part B), 234−241.

(28) Hooft, A. M., Maki, E. J., Cox, K. K., and Baker, J. E. (2007) An accelerated state of myosin-based actin motility. *Biochemistry 46*, 3513−3520.

(29) Harris, D. E., and Warshaw, D. M. (1993) Smooth and skeletal muscle myosin both exhibit low duty cycles at zero load in vitro. *J. Biol. Chem. 268*, 14764−14768.

(30) Schlager, G. (1999) *Statistics for Biochemists*, Madeline Press, Princeville, HI.

(31) Mathews, J. H., and Fink, K. K. (2004) *Numerical Methods Using Matlab*, 4th ed., Prentice-Hall Inc., Upper Saddle River, NJ.

(32) Harris, D. E., Stromski, C. J., Hayes, E., and Warshaw, D. M. (1995) Thiophosphorylation independently activates each head of smooth muscle myosin in vitro. *Am. J. Physiol. 269*, C1160−C1166.

(33) Harris, D. E., Work, S. S., Wright, R. K., Alpert, N. R., and Warshaw, D. M. (1994) Smooth, cardiac and skeletal muscle myosin force and motion generation assessed by cross-bridge mechanical interactions in vitro. *J. Muscle Res. Cell Motil. 15*, 11−19.

(34) Sellers, J. R., Chock, P. B., and Adelstein, R. S. (1983) The apparently negatively cooperative phosphorylation of smooth muscle myosin at low ionic strength is related to its filamentous state. *J. Biol. Chem. 258*, 14181−14188.

(35) Mabuchi, Y., Mabuchi, K., Stafford, W. F., and Grabarek, Z. (2010) Modular structure of smooth muscle myosin light chain kinase: Hydrodynamic modeling and functional implications. *Biochemistry 49*, 2903−2917.

(36) Birkhoff, G. D. (1931) Proof of the Ergodic Theorem. *Proc. Natl. Acad. Sci. U.S.A. 17*, 656−660.

(37) Knight, A. E., Veigel, C., Chambers, C., and Molloy, J. E. (2001) Analysis of single-molecule mechanical recordings: Application to acto-myosin interactions. *Prog. Biophys. Mol. Biol. 77*, 45−72.